Signatures of topological defects

Veniamin Berezinsky
INFN, Laboratori Nazionali del Gran Sasso, I-67010 Assergi (AQ), Italy
and Institute for Nuclear Research, Moscow, Russia

Pasquale Blasi
Department of Astronomy & Astrophysics and Enrico Fermi Institute, The University of Chicago,
5640 South Ellis Avenue, Chicago, Illinois 60637

Alexander Vilenkin
Institute of Cosmology, Department of Physics and Astronomy, Tufts University, Medford, Massachusetts 02155
(Received 11 May 1998; published 27 October 1998)

We argue that due to various restrictions cosmic strings and monopole-string networks are not likely to produce the observed flux of ultrahigh energy cosmic rays (UHECR). Among the topological defects studied so far, the most promising UHECR sources are necklaces and monopolonia. Other viable sources which are similar to topological defects are relic superheavy particles. All these sources have an excess of pions (and thus photons) over nucleons at production. We demonstrate that in the case of necklaces the diffuse proton flux can be larger than the photon flux, due to absorption of the latter on the radio background, while monopolonia and relic particles are concentrated in the galactic halo, and the photon flux dominates. Another signature of the latter sources is anisotropy imposed by the asymmetric position of the Sun in the galactic halo. In all cases considered so far, including necklaces, photons must be present in ultrahigh energy radiation observed from topological defects, and experimental discrimination between photon-induced and proton-induced extensive air showers can give a clue to the origin of ultrahigh energy cosmic rays. [S0556-2821(98)09220-0]

PACS number(s): 98.80.Cq, 11.27.+d, 98.70.Sa

I. INTRODUCTION

The observation of cosmic ray particles with energies higher than 10^{11} GeV [1] gives a serious challenge to the known mechanisms of acceleration. The shock acceleration in various astrophysical objects typically gives a maximal energy of accelerated protons less than $(1-3)\times 10^{10}$ GeV [2] (see however [3]). The unipolar induction can provide a maximum energy of 1×10^{11} GeV only for extreme values of the parameters [4]. Much attention has recently been given to acceleration by ultrarelativistic shocks [5,6]. The particles here can gain a tremendous increase in energy, equal to Γ^2, at a single reflection, where Γ is the Lorentz factor of the shock. However, it is known (see, e.g., the simulation for pulsar relativistic wind in [7]) that particles entering the shock region are captured there or at least have a small probability to escape.

Topological defects (TD) (for a review see [8]) can naturally produce particles of ultrahigh energies (UHE) well in excess of those observed in cosmic rays (CR). In most cases the problem with topological defects is not the maximum energy but the fluxes. However, in some cases the predicted fluxes are comparable with observations.

Usually, UHE particles appear at the decays of superheavy (SH) particles produced by TD. (We shall refer to these SH particles as *X* particles.) Examples discussed in the literature include ejection of X particles from superconducting strings, emission of X particles from cusps or intersections of ''ordinary'' strings, and production of such particles in monopole-antimonopole annihilations. Metastable SH particles can also be relics of an earlier epoch, produced by a thermal or some other mechanism in the early Universe.

A rather exceptional mechanism of UHE particle production is given by radiation of accelerated monopoles connected by strings. In this case a monopole can radiate gluons with very large Lorentz factors and with virtualities of the order of the monopole acceleration.

A common signature of all extragalactic UHE cosmic rays (UHECR) is the Greisen-Zatsepin-Kuzmin (GZK) cutoff [9]. It reveals itself as a steepening of the spectrum of UHE protons and nuclei due to their interaction with microwave radiation. The steepening starts at $E\approx 3\times 10^{10}$ GeV. Apart from this steepening there is another signature of interaction of extragalactic CR with microwave radiation: a bump in the spectrum preceeding the cutoff. The bump is a consequence of the proton number conservation in the spectrum: protons loose energy and are accumulated before the cutoff.

In this paper we will discuss the signatures of UHECR from TD distinguishing them from particles produced by astrophysical accelerators.

We will confine ourselves here to the case of the conventional primary particles, protons and photons, and will not consider the other UHE signal carriers discussed in the literature such as neutrinos [10,11], lightest supersymmetric particles [12,13], relativistic monopoles [14] and vortons [15].

Throughout the paper we shall use the following numerical values and abbreviations: the dimensionless Hubble constant $h=0.65$, the cold dark matter density in terms of critical density $\Omega_{CDM}=0.2h^2$, the size of dark matter halo $R_h=100$ kpc, UHECR for ultra high energy cosmic rays and UHE for ultra high energy, TD for topological defect, SH for

superheavy, CDM for cold dark matter, SUSY for supersymmetry, LLA for leading logarithmic approximation, AGN for active galactic nucleus, and GC and AC for galactic center and anticenter, respectively.

II. CONSTRAINTS AND SIGNATURES

A common characteristic feature of UHE particle production in TD is an excess of pions over nucleons [16,17]. As a result in many cases the observed UHE gamma-ray flux dominates over proton flux and it makes γ/p ratio ''a diagnostic tool'' [16] for TD. We shall discuss this signature quantitatively for various sources, such as cosmic necklaces, monopolonia and superheavy relic particles.

An excess of photons over protons *at generation* is present in all known mechanisms of high energy particle generation: decay of SH particles produced by strings and cusps, annihilation of monopoles and radiation of UHE particles by accelerated monopoles. The order of magnitude of this excess can be estimated from the ratio of energy transferred to pions and nucleons in the QCD cascade. For example, N/π ratio for the decay $Z^0 \to hadrons$ is about 5% (N includes $p,\bar{p},n,\bar{n}$ and π—charged and neutral pions). To estimate γ/N-ratio at energy of interest, one should take into account two photons produced by each π^0-decay, the fraction (1/3) of neutral pions relative to all pions and the energy spectrum of produced hadrons. It gives roughly $\gamma/N \sim 10$ at production. However, in the observed diffuse flux at $E > 10^6$ GeV the proton component[1] can dominate because of the strong absorption of high energy photons on the background photon radiation. UHE photons are absorbed mainly on radio background [18,19] and the absorption length is sensitive to low-frequency cutoff in this background.

The pion dominance of hadron production by TD has two consequences. (i) A large part of hadron energy is transferred, due to pion decays, to an electromagnetic cascade. This can be used to derive an upper bound on the UHE proton flux. (ii) TD localized inside the sphere of gamma-ray absorption give a direct flux of UHE photons at the Earth, producing thus an observable anisotropy.

The e-m cascade upper limit on UHECR arises due to cascading of electrons and photons in the Universe down to the observed energies 10 MeV–100 GeV. The flux of the cascade photons at these energies must be lower than the extragalactic flux measured by Energetic Gamma Ray Experiment Telescope (EGRET) [20]. The cascade photon flux is below the EGRET extragalactic flux at 10 MeV–100 GeV if the energy density of the cascade photons is $\omega_{cas} \leqslant 2 \times 10^{-6}$ eV/cm^3. This result follows from Monte Carlo simulation in [21,22] and from our own estimates based on analytic calculations in [4,23]). This limit (which will be used in our calculations) is rather rigorous: due to uncertainties in infra-red flux and intergalactic magnetic field the allowed density of the cascade radiation can be as high as $(3-5)\times 10^{-6}$ eV/cm^3.

The energy density of e-m cascades can be readily calculated as

$$\omega_{cas} = \frac{1}{2} f_\pi m_X \int_0^{t_0} dt \dot{n}_X(t)(1+z)^{-4}, \tag{1}$$

where $\dot{n}_X(t)$ is the rate of X-particle production at the epoch t (redshift z), $t_0 = 2.06\times 10^{17} h^{-1}$ s is the age of the Universe, h is the dimensionless Hubble constant, f_π is the fraction of energy transferred to pions at the decay of X particle, and 1/2 takes into account that half of this energy goes into e-m cascade. One can parametrize the effect of the evolution of TD on X-particle production as [24] $\dot{n}_X(t) = \dot{n}_X(t_0)(t/t_0)^{-m}$. In most cases, e.g., ordinary strings, monopolonium, and necklaces, $m=3$. In this case the integral in Eq. (1) reduces to $\int dz/(1+z)^2$, i.e., the evolutionary effects are absent. In the case of superconducting strings, m is model-dependent and it can be $m=4$ or larger. Weak cosmological effects are present in this case.

With ω_{cas} from Eq. (1) and the diffuse proton flux being determined by $f_N \dot{n}_X(t_0)$, where f_N is a fraction of m_X transferred to UHE nucleons, one can obtain an upper bound on the diffuse flux of UHE (for another approach see [21]).

It is easy to generalize the calculations above to the case when X particles are produced with a large Lorentz factor Γ.

Another general restriction on TD models is given by the distance between the topological defects, D. There are three distance scales in our problem: the distance between TD, D, the photon absorption length, $R_\gamma(E)$, and the proton attenuation length, $R_p(E) = c(E^{-1}dE/dt)^{-1}$, where dE/dt is the energy loss of UHE proton on microwave radiation. We shall analyze the case $R_\gamma < R_p$, though at very high energies, $E > 10^{12}$ GeV, they can be comparable.

For TD with $D > R_p(E)$ the diffuse flux at a representative point between TD is exponentially suppressed. For a power-law generation spectrum with exponent γ_g and the distance $D/2$ to the nearest source, the suppression factor for rectilinear propagation is

$$\exp(-(\gamma_g - 1)D/2R_p(E)). \tag{2}$$

In the case of diffusive propagation, $D/2$ should be replaced by the propagation time. Such TD are disfavored as sources of UHECR, because their spectrum either has an exponential cutoff at energy where $R_p(E) < D$ or, in case of accidental proximity of a source, the flux is anisotropic. The anisotropy can be estimated as $\delta \sim l/2ct$, where l is the distance to the source and t is the propagation time.

In the other extreme case, $D < R_\gamma(E)$, a TD located inside the photonic sphere R_γ creates a direct UHE photon flux, $F_\gamma = Q_\gamma/4\pi r^2$ at the point of observation. The produced extensive atmospheric showers (EAS) can be identified as photon-induced EAS in the direction of the source.

The *proton-induced* showers can dominate in the case $R_\gamma(E) < D < R_p(E)$. The sources might be absent inside the photonic sphere with radius R_γ and thus, if magnetic field is

[1]Here and below we shall refer to the $p+\bar{p}$ diffuse flux from TD as to *proton* flux.

strong enough, no source is seen directly. The proton spectrum exhibits the usual GZK cutoff, due to energy losses of the nucleons produced by the sources beyond the distance R_p. Since at extremely high energies R_p and R_γ are not much different, the number of sources inside the GZK sphere of radius R_p is not large and some anisotropy is expected.

Finally let us turn to the case $D \ll R_\gamma(E)$. Generically, this is a case of uniformly distributed sources. The proton showers dominate when $R_p(E) > R_\gamma(E)$; their spectrum has the usual GZK cutoff. A certain fraction of showers, $\sim R_\gamma/R_p$, are the photon-induced ones, and they correspond to the direct arrival of the photons. The γ/p-ratio depends thus on the calculations of attenuation lengths of photons and protons. We shall analyze this case quantitatively.

A special situation arises when the sources are concentrated in the galactic halo. This happens in the case of relic superheavy particles [25]. Here we point out that the same phenomenon of galactic enhancement occurs for monopolonium and decaying vortons.

The energy losses and absorption are negligible for the halo model and thus photons strongly dominate.

Another signature of this model was indicated recently in [26]: because of asymmetric position of the Sun in the galactic halo, there is a considerable anisotropy of UHE photon flux.

III. FLUXES

In this section we shall give the formulas for UHE proton and photon fluxes from extragalactic space and from the halo (for the case of SH relic particles and monopolonia). The basic quantity which determines these fluxes is the rate of X-particles production $\dot{n}_X$. In the case of an extragalactic flux we assume that sources are uniformly distributed in space and $\dot{n}_X$ does not depend on time. For the galactic model we assume that $\dot{n}_X$ is a function of the distance from galactic center R.

X particles can be produced by TD at rest or with a Lorentz factor Γ. The decay of an X particle results in a parton cascade. The energy spectrum of hadrons outside the confinement radius is described by fragmentation functions $W_N(x,m_X)$ for nucleons and $W_\pi(x,m_X)$ for pions, where $x = 2E/m_X$ and E is the energy of a proton or a photon. For fragmentation functions we use the supersymmetric generalization [28] of the LLA limiting spectrum of QCD cascade [27] normalized by the fraction of energy transferred to the nucleons f_N, and pions f_π, respectively:

$$\int_0^1 dx x W_i(x,m_X) = 2 f_i \tag{3}$$

with $i = N, \pi$. In all calculations below we shall use $f_\pi \approx 0.5$, as suggested by calculations [13], which show that about half of energy of SUSY-QCD cascade is taken away by neutralinos and high-energy leptons. For the ratio f_N/f_π we shall use 0.05 inspired by data on Z^0 decay. The SUSY-QCD fragmentation function considerably differs from that of ordinary QCD [28]: the maximum of the Gaussian peak is shifted towards smaller x, and the peak is much higher, while at larger x SUSY-QCD spectrum is below the ordinary QCD spectrum. Since ω_{cas} is determined by large x, *there are more UHE particles at fixed* ω_{cas} *in case of SUSY-QCD fragmentation function, as compared with ordinary QCD spectrum.*

As it is discussed in [27–29] the normalization of analytic solutions by conservation of total energy, results in large uncertainty in the normalization constant. On the other hand, the ordinary QCD spectrum (used, e.g., in [29]) has *the shape* of the spectrum much different from SUSY-QCD spectrum. One needs SUSY-QCD Monte Carlo simulation for properly normalized SUSY-QCD spectrum.

The spectra of extragalactic UHE protons and photons can be calculated as

$$I_p^{extr}(E) = \frac{\dot{n}_X^{extr} c}{2\pi m_X} \int_0^\infty dt W_N(x_g, m_X) \frac{dE_g(E,t)}{dE}, \tag{4}$$

$$I_\gamma^{extr}(E) = R_\gamma(E) \frac{\dot{n}_X^{extr}}{\pi m_X} \int_{2E/m_X}^1 \frac{dx}{x} W_{\pi^0}(x, m_X), \tag{5}$$

$$\frac{dE_g(E,z_g)}{dE} = (1+z_g) \exp\left(\int_0^{z_g} \frac{dz}{H_0} (1+z)^{1/2} \times (db(E,0)/dE)_{E=E_g(z)} \right), \tag{6}$$

where $x_g = 2E_g/m_X$ and $E_g(E,t)$ is the energy of generation at time t for a proton with energy E now. The energy E_g is determined by proton energy losses on microwave radiation $dE/dt = b(E,z)$ and due to redshift. The expression dE_g/dE, given by Eq. (6), is taken from [30].

The photon absorption length, $R_\gamma(E)$, at very high energies is determined mostly by pair production on radio background. For our calculations we use the absorption lengths from [19]. The photon absorption lengths from [18] and [19] are plotted in Fig. 1.

As one can see from Eq. (4), the proton flux is calculated with recoil protons taken into account, while for photons we neglect multiplication due to cascade on background photons. The reason is that electron-positron pairs produced as a result of absorption of primary photons on radio-photons, are losing their energies on radiobackground practically continuously and most of their energy is lost before a collision with a microwave photon—the process responsible for the cascade development.

The ratios $\gamma/p = I_\gamma(E)/I_p(E)$ as determined by Eqs. (4), (5) are plotted in Fig. 2 as functions of energy for two extreme cases of absorption length from [19]. One can see that even for the exceptional case of low γ/p ratio considered here ($D \ll R_\gamma$), it becomes appreciable, $0.5 \leqslant \gamma/p \leqslant 2.5$, at energy 3×10^{11} GeV and increases further with energy.

Let us consider now the halo model. In cases of SH relic particles [25] and monopolonia, their density is everywhere proportional to the density of cold dark matter (CDM). Thus,

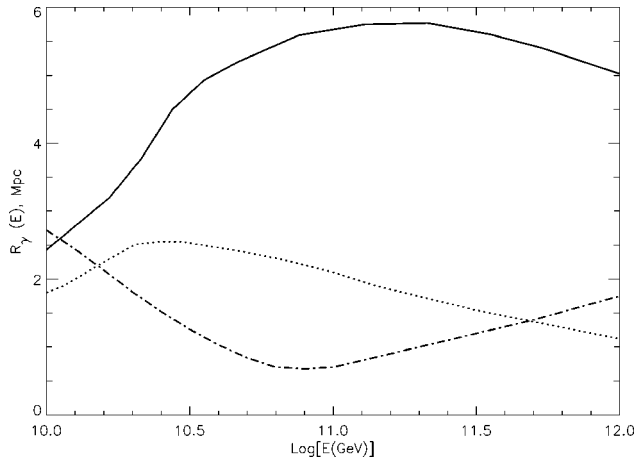

FIG. 1. Gamma-ray absorption length as a function of energy. The solid line and the dotted line reproduce the upper and lower case of Ref. [19], while the dash-dotted line is taken from Ref. [18] and drawn here for comparison.

the ratio of the rates of X-particle production in the halo, $\dot{n}_X^h(r_\odot)$, and in extragalactic space, $\dot{n}_X^{extr}$, is given by

$$\frac{\dot{n}_X^h(r_\odot)}{\dot{n}_X^{extr}} = \frac{\rho_{CDM}^h(r_\odot)}{\Omega_{CDM}\rho_{cr}}, \tag{7}$$

where $r_\odot$ is the distance between the Sun and the galactic center, Ω_{CDM} is the CDM density in the extragalactic space in units of critical density ρ_{cr} and $\rho_{CDM}^h(r_\odot) \approx 0.3$ GeV/cm^3 is the local CDM density in the halo.

The fluxes of UHE protons ($i=p$) and photons ($i=\gamma$) from the halo can be calculated as

$$I_i^h(E) = \frac{W_i(E)}{4\pi}\int_0^\pi \cos\theta d\cos\theta \int_0^{r_{max}} dr \dot{n}_X^h(R), \tag{8}$$

where θ is an angle relative to the direction of GC and

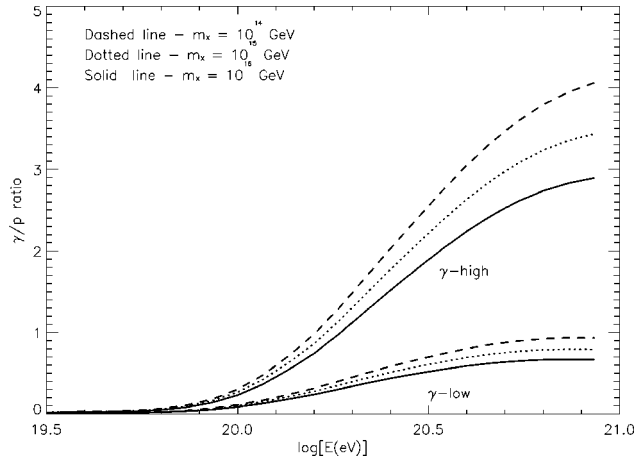

FIG. 2. The γ/p ratio for different values of m_X (indicated in the figure) as a function of the gamma-ray energy. High (γ-high) and low (γ-low) photon fluxes correspond to two extreme cases of gamma-ray absorption from [19].

$$r_{max}(\theta) = r_\odot \cos\theta + \sqrt{R_h^2 - r_\odot^2 \sin^2\theta}.$$

The rate of particle production, $\dot{n}_X^h(R)$, is parametrized here as density of DM [31],

$$\dot{n}_X^h(R) = \frac{\dot{n}_0^h}{(R/r_0)^\gamma [1+(R/r_0)^\alpha]^{(\beta-\gamma)/\alpha}}, \tag{9}$$

where $\dot{n}_0^h$ is the normalizing rate, R is the distance from the galactic center, $\alpha,\beta,\gamma=(2,2,0)$ correspond to isothermal profile, $\alpha,\beta,\gamma=(2,3,0.2)$ gives, according to [31], the best fit to observational data, and $\alpha,\beta,\gamma=(1,3,1)$ describes the numerical simulations of Ref. [32].

The functions $W_p(E)$ and $W_\gamma(E)$ in Eq. (8) can be given in terms of fragmentation functions, $W_N(x,m_X)$ and $W_{\pi^0}(x,m_X)$, as

$$W_p(E) = \frac{1}{m_X} W_N(x,m_X),$$

$$W_\gamma(E) = \frac{2}{m_X}\int_{2E/m_X}^1 \frac{dx}{x} W_{\pi^0}(x,m_X). \tag{10}$$

Relic particles and monopolonia fill also extragalactic space with space density proportional to $\Omega_{CDM}\rho_{cr}$. The decay rate $\dot{n}_X^{extr}$ is given by Eq. (7) and the fluxes by Eqs. (4) and (5).

IV. SOURCES

The following topological defects have been discussed as potential sources of UHE particles: (i) superconducting strings [33]; (ii) ordinary strings [34], including the cusp radiation [35]; (iii) networks of monopoles connected by strings [36,37]; (iv) necklaces [38], hybrid topological defects, where each monopole is attached to two strings; (v) magnetic monopoles, or more precisely bound monopole-antimonopole pairs (monopolonium [39,40]); (vi) vortons [41]: small loops of superconducting string stabilized by their angular momentum.

Finally we include in this list SH quasistable relic particles produced in the early Universe [42,25,43–45,29]. Here we shall apply the criteria discussed in the previous section to each of these sources.

i. Superconducting strings. Superconducting strings produce SH particles when the electric current in the strings reaches the critical value, $i=i_c$. In some scenarios, e.g., [46] where the current is induced by primordial magnetic field, the critical current produces strong magnetic field, in which all high energy particles degrade catastrophically in energy [47]. However, for ac currents there are portions of the string with large electric charge and small current. High energy particles can escape from there.

Large ac currents can be induced in string loops as they oscillate in galactic or extragalactic magnetic fields. Even if the string current is typically well below critical, supercritical currents can be reached in the vicinity of cusps, where the string shrinks by a large factor and density of charge carriers

is greatly enhanced. In this case, SH particles are emitted with large Lorentz factors.

Loops can also acquire dc currents at the time of formation, when they are chopped off the infinite strings. As the loops lose their energy by gravitational radiation, they shrink, the dc currents grow, and eventually become overcritical. There could be a variety of astrophysical mechanisms for excitation of the electric current in superconducting strings, but for all mechanisms considered so far the flux of UHE particles is smaller than the observed flux [48]. However, the number of possibilities to be explored here is very large, and more work is needed to reach a definitive conclusion.

ii. Ordinary strings. There are several mechanisms by which ordinary strings can produce UHE particles.

For a special choice of initial conditions, an ordinary loop can collapse to a double line, releasing its total energy in the form of X particles [34]. However, as noted in [34], the probability of this mode of collapse is extremely small, and its contribution to the overall flux of UHE particles is negligible.

String loops can also produce X particles when they self-intersect (e.g., [49]). Each intersection, however, gives only a few particles, and the corresponding flux is very small [50].

Superheavy particles with large Lorentz factors can be produced in the annihilation of cusps, when the two cusp segments overlap [35]. The energy released in a single cusp event can be quite large, but again, the resulting flux of UHE particles is too small to account for the observations [55,50].

One effect which was not considered in [50] and [35] could increase the production of UHE particles [51,34]. As a nonintersecting closed loop oscillates and radiates away its energy, the loop configuration is gradually changing. After the loop has lost a substantial part of its energy, it is likely to self-intersect and fragment into several smaller loops. These daughter loops will go through the same cycle, and the process will continue until the size of the fragments becomes comparable to the string thickness, at which point the fragment loops disintegrate into relativistic particles. UHE radiation is also emitted from cusps on the daughter loops.

The process of loop fragmentation is not well understood. We do not know, for example, the number and size distribution of the fragments. The only numerical simulation of the fragmentation process that we are aware of, Ref. [52], used initial loops of arbitrary shape, and it is not at all clear that the results are relevant for loops produced in a realistic evolving network. To address this problem, we used a simple analytic model (see Appendix A) which assumes that, in each round of fragmentation, a loop looses a fixed fraction $(1-f_1)$ of its energy to gravitational waves and breaks into a fixed number (N_1+1) of daughter loops of roughly equal size. The daughter loops move with Lorentz factors Γ_1 in the rest frame of the parent loop. This model, which is similar to that introduced in Ref. [51], is analyzed in Appendix A, with the conclusion that, for reasonable values of the parameters f_1, N_1, and Γ_1, the UHECR flux from fragmenting loops is still too small. While these results are suggestive, a detailed numerical simulation of loop fragmentation with gravitational back-reaction will be needed to reach a more definitive conclusion. However, there is one general argument against this model of UHECR production. In the chain of fragmentation the Lorentz factor of the daughter loops increases multiplicatively, e.g., in our model as Γ_1^n, and at the moment of collapse, reaches a large value. The large maximum energy of X particle results, for the observed UHECR flux, in an unacceptably high cascade gamma radiation. This fact, observed in all calculations (see for example [21]) is easy to understand. The total energy of decaying X-particle is released mostly in the particles of highest energies. When one fixes the flux of UHECR at a given energy, e.g., $E=1.0\times10^{20}$ eV, and increases E_{max}, the energy transferred to e-m cascades increases. This argument works especially strongly in case of cusps, where the Lorentz factor can reach tremendous values, e.g., $\Gamma\sim10^{15}-10^{17}$ in [35].

It has been recently argued [53] that long strings lose most of their energy not by production of closed loops, as it is generally believed, but by direct emission of heavy X particles. If correct, this claim will change dramatically the standard picture of string evolution. It has been also suggested that the decay products of particles produced in this way can explain the observed flux of UHE cosmic rays [53,54]. However, we are not convinced that the conclusions of Ref. [53] are justified. In fact, we believe that numerical simulations described in [53] allow an alternative interpretation. The initial string separation in these simulations is comparable to the string thickness. As a result, string intersections and reconnections can generate a large amount of energy in the form of short-wavelength perturbations on the strings. These perturbations may then be released in the form of particles from portions of the string that undergo contraction in the course of the following evolution.

Even if the conclusions of [53] were correct, the particle production mechanism suggested in that paper cannot explain the observed flux of UHE particles. If particles are emitted directly from long strings, then the distance between UHE particle sources is of the order of the Hubble distance, $D\sim t_0\gg R_p$. According to the discussion in the preceding section, the flux of UHE particles in this case is exponentially suppressed, or, in the case of accidental proximity of a string to the observer, the flux is strongly anisotropic. A fine-tuning in the position of the observer is needed to reconcile both requirements, because long strings are separated by a Hubble distance.

iii. Network of monopoles connected by strings. The sequence of phase transitions

$$G\rightarrow H\times U(1)\rightarrow H\times Z_N \tag{11}$$

results in the formation of monopole-string networks in which each monopole is attached to N strings. Most of the monopoles and most of the strings belong to one infinite network. The evolution of networks is expected to be scale-invariant with a characteristic scale

$$d=\kappa t, \tag{12}$$

where $\kappa=$const. The scale d gives the average distance between monopoles and the typical length of string segments. Each string attached to a monopole pulls it with a force equal

to the string tension, $\mu \sim \eta_s^2$, where η_s is the symmetry breaking VEV of strings. The monopoles are accelerated and radiate gauge quanta at the rate

$$\frac{dE}{dt} \sim \frac{h^2}{6\pi} a^2 \sim \frac{\mu^2}{g^2 m^2}, \tag{13}$$

where $h \sim 2\pi/g$ and m are the monopole charge and mass, respectively, g is the gauge coupling and $a \sim \mu/m$ is the monopole acceleration. The GUT monopole has magnetic and chromomagnetic charges, $h_m \sim 2\pi/e$ and $h_s \sim 2\pi/3g_s$, respectively, where e is the e-m coupling constant and g_s is the color coupling constant. From Eq. (13) it follows that the energy losses are dominated by e-m radiation. Then a simple energy balance analysis gives the value of κ in Eq. (12) [36],

$$\kappa \sim \mu/e^2 m^2. \tag{14}$$

The energy of gauge quanta (practically photons and gluons) radiated by monopoles can be estimated assuming a rough energy equipartition between the monopole and string subsystems. Then the monopoles have a typical energy $E \sim \mu d$ and Lorentz factor $\Gamma_M \sim \mu d/m$. If the mass of gauge quanta (or the virtuality Q^2 in the case of gluon) is smaller than the monopole acceleration a, the typical energy of gauge quanta is $\epsilon \sim \Gamma_M a$ [37]; otherwise the production rate of massive gauge quanta is exponentially suppressed. Gluon production is also suppressed unless $a > \Lambda_{QCD}$, that is,

$$\mu/m > 1 \text{ GeV}. \tag{15}$$

Thus we have for both photons and gluons with $Q^2 \leqslant a^2$

$$\epsilon \sim (\mu/em^2)^2 \mu t. \tag{16}$$

The production rate (per unit volume) of these particles is

$$\dot{n}_i \sim n_M(t) \epsilon^{-1} (dE/dt)_i, \tag{17}$$

where subscript i runs through γ for photon and g for gluon. In particular for gluons we obtain

$$\dot{n}_g \sim \frac{1}{4} \frac{e^8}{g_s^2} \left(\frac{m^2}{\mu t} \right)^4. \tag{18}$$

Let us assume that each gluon with energy ϵ fragments to hadrons with a power-law energy spectrum KE^{-q}. If we take $q = 1.5$ the cascade limit will be somewhat weaker than in the case of a more realistic QCD fragmentation function. Let us proceed with this favorable case. Using the normalized fragmentation function

$$N_p(\epsilon, E) dE = \frac{f_N}{2} \sqrt{\epsilon} E^{-1.5} dE \tag{19}$$

and the rate of gluon production $\dot{n}_g$ given by Eq. (18), one obtains for the diffuse proton flux

$$I_p(E) dE = \frac{1}{32\pi} f_N \frac{e^8}{g_s^2} \frac{R_p(E)}{t_0^4} \left(\frac{m^2}{\mu} \right)^4 \left(\frac{E}{\epsilon} \right)^{-1.5} \frac{dE}{\epsilon}. \tag{20}$$

The cascade energy density is determined by the e-m radiation of monopoles and can be estimated as

$$\omega_{cas} = 4\pi e^4 \frac{m^4}{\mu} \frac{1}{t_0^2}. \tag{21}$$

Requiring that $\omega_{cas} \leqslant \omega_{obs}$, the proton flux at energy $E \sim 1 \times 10^{11}$ GeV is bounded by

$$E^3 I_p(E) < 3.7 \times 10^{14} \mu_6^{-1} \text{ m}^{-2} \text{ s}^{-1} \text{sr}^{-1} \text{ eV}^2, \tag{22}$$

where $\mu_6 = \mu/10^6$ GeV^2. The symmetry breaking scale of strings is unlikely to be below the electroweak scale, $\mu > 10^4$ GeV^2, and the flux (22) is considerably lower than that observed.

iv. Necklaces. Necklaces are hybrid TD corresponding to the case $N = 2$ in Eq. (11), i.e., to the case when each monopole is attached to two strings. This system resembles ''ordinary'' cosmic strings, except the strings look like necklaces with monopoles playing the role of beads. The evolution of necklaces depends strongly on the parameter

$$r = m/\mu d, \tag{23}$$

where d is the average separation between monopoles and antimonopoles along the strings. As it is argued in Ref. [38], necklaces might evolve to configurations with $r \gg 1$, though numerical simulations are needed to confirm this conclusion. Monopoles and antimonopoles trapped in the necklaces inevitably annihilate in the end, producing first the heavy Higgs and gauge bosons (X particles) and then hadrons. The rate of X-particle production is easy to estimate as [38]

$$\dot{n}_X \sim \frac{r^2 \mu}{t^3 m_X}. \tag{24}$$

Using Eqs. (4) and (5) one can calculate the fluxes of UHE protons and gammas taking into account the restriction due to cascade radiation

$$\omega_{cas} = \frac{1}{2} f_\pi r^2 \mu \int_0^{t_0} \frac{dt}{t^3} \frac{1}{(1+z)^4} = \frac{3}{4} f_\pi r^2 \frac{\mu}{t_0^2}. \tag{25}$$

The separation between necklaces is given by [38] $D \sim r^{-1/2} t_0$ for large r. Since $r^2 \mu$ is limited by cascade radiation, Eq. (25), one can obtain a lower limit on the separation D between necklaces as

$$D \sim \left(\frac{3 f_\pi \mu}{4 t_0^2 \omega_{cas}} \right)^{1/4} t_0 > 10 (\mu/10^6 \text{ GeV}^2)^{1/4} \text{ kpc}, \tag{26}$$

where we used $f_\pi \approx 0.5$. Another (weaker) constraint on the parameters of the model follows from the condition $d \geqslant \delta_s$, where $\delta_s \sim 1/(e\eta_s)$ is the string width and η_s is the string symmetry breaking scale. This condition gives r_{max}

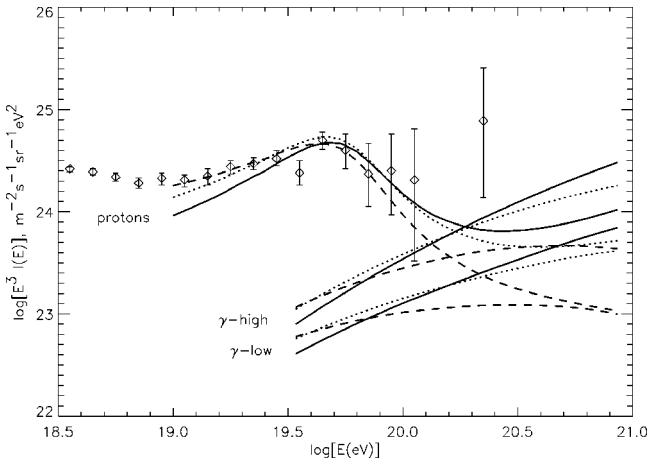

FIG. 3. Proton and gamma-ray fluxes from necklaces. High (γ-high) and low (γ-low) photon fluxes correspond to two extreme cases of gamma-ray absorption from [19]. The fluxes are given for $m_X=1\times10^{14}$ GeV (dashed lines), $m_X=1\times10^{15}$ GeV (dotted lines), and $m_X=1\times10^{16}$ GeV (solid lines). The fluxes are normalized to the observed data.

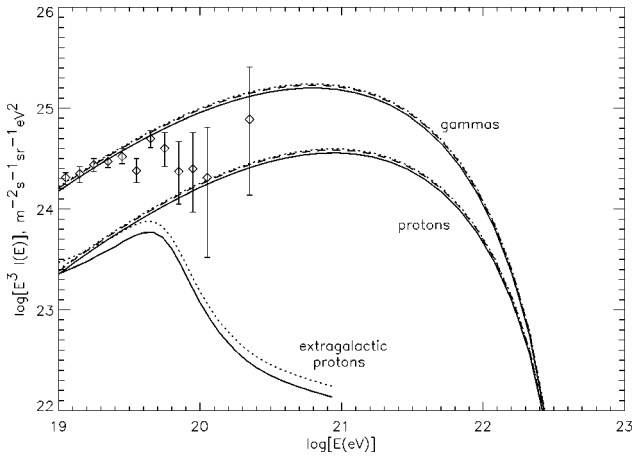

FIG. 4. Predicted fluxes from relic SH particles ($m_X=1\times10^{14}$ GeV) or from monopolonia producing X-particles with the same masses: nucleons from the halo (curves labelled as ''protons''), gamma-rays from the halo (curves labelled ''gammas''), and extragalactic protons (as indicated). The solid, dotted and dashed curves correspond to $(\alpha,\beta,\gamma)=(2,2,0),(2,3,0.2)$, and $(1,3,1)$ respectively (see text).

$\sim\eta_m/\eta_s$, where η_m is the monopole symmetry breaking scale. For $\eta_m\sim10^{16}$ GeV and $\eta_s\sim10^3$ GeV, one obtains $r_{max}\sim10^{13}$, which corresponds to $D_{min}\sim1$ kpc.

Thus, necklaces can give a realistic example of the case $D\ll R_\gamma$, when the Universe is uniformly filled by the sources. The proton-induced EAS from necklaces strongly dominate over those induced by photons at all energies except $E>3\times10^{11}$ GeV (see Fig. 3), where photon-induced showers can comprise an appreciable fraction of the total rate.

The spectra of protons and photons from necklaces are shown in Fig. 3. The calculations were performed with the help of Eq. (4) and Eq. (5) using the SUSY-QCD fragmentation functions. The dashed, dotted, and solid lines correspond to the masses of X particles 10^{14} GeV, 10^{15} GeV, and 10^{16} GeV, respectively. The values of $r^2\mu$ used to fit these curves to the data are 7.1×10^{27} GeV^2, 6.0×10^{27} GeV^2, and 6.3×10^{27} GeV^2, respectively. They correspond to the cascade density ω_{cas} equal to 1.5×10^{-6} eV/cm^3, 1.2×10^{-6} eV/cm^3, and 1.3×10^{-6} eV/cm^3, respectively, all less than the allowed cascade energy density for which we adopt the conservative value $\omega_{cas}=2\times10^{-6}$ eV/cm^3.

The absorption of gamma-radiation on the radio background is taken according with the upper and lower limits of [19], shown in Fig. 2. The agreement with observational data at the highest energies is improved when the photon flux is added to the proton flux.

Two following effects are expected to improve the agreement with the data at $E>1\times10^{11}$ GeV.

The fluctuations in energy losses increase the fluxes. This effect is significant when the fraction of energy lost in one collision becomes appreciable, i.e., at $E>1\times10^{11}$ GeV. This effect can be accounted for in Monte Carlo simulations.

The local enhancement of the density of sources, e.g., within local supercluster (LS), makes the spectrum at $E>3\times10^{10}$ GeV flatter (see calculations in [56]). The accumulation of necklaces within LS is expected for large r. Indeed, for sufficiently large r, the typical velocity of necklaces $v=c/\sqrt{r}$ is less than the escape velocity from the local supercluster and thus necklaces are confined within LS. For $r>10^7$ necklaces can also cluster on the galactic scale.

For energy lower than 1×10^{10} GeV we assume the presence of another component with a cutoff at $E\sim1\times10^{10}$ GeV. It can be generated, for example, by jets from AGN [57], which naturally have a cutoff at this energy.

v. Monopolonium and SH relic particles. These two sources exhibit the same clustering property: they act as nondissipative matter which clusters in the Universe in the same way as cold dark matter. As a result the density of these particles in the galactic halo is enhanced according to Eq. (7).[2] The spectra of UHE protons and photons from decays of relic particles in the halo are calculated using Eq. (8) for the different distributions of X particles in the halo given by Eq. (9). The results are displayed in Fig. 4. The mass of X particle is $m_X=1\times10^{14}$ GeV. The solid, dotted, and dashed curves correspond to the distribution (9) with (α,β,γ) equal to (2,2,0), (2,3,0.2), and (1,3,1), respectively. The shape of the spectra is naturally the same for all three curves. Since we normalize the spectra by the value $\dot{n}_0^h$ to fit the observa-

[2]Clustering of free monopoles in the galactic halo has been briefly discussed in Ref. [26]. The authors argue that the monopole density n_M is proportional to the dark matter density and that the X particle production rate due to monopole-antimonopole annihilation is $\dot{n}_X\propto n_M^2$. There are, however, some problems with this picture. The motion of free monopoles is strongly affected by the galactic magnetic field, and their density is not likely to follow that of CDM. Moreover, the probability for annihilation of free monopoles in the galactic halo is extremely small, and the resulting flux of cosmic rays is negligible for all reasonable values of the monopole density n_M.

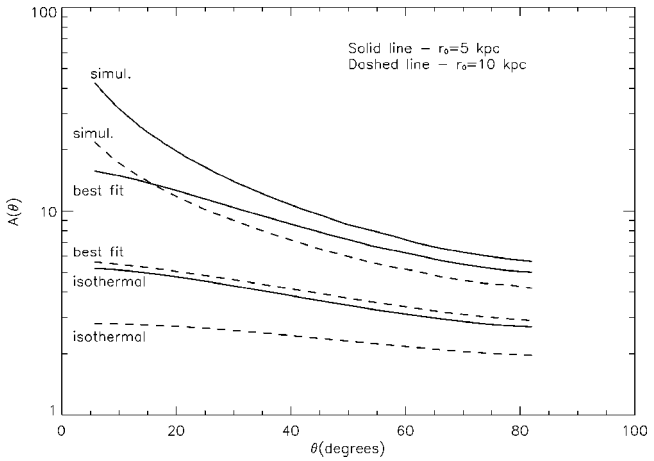

FIG. 5. Anisotropy $A(\theta)$ as a function of the angle θ. $A(\theta)$ is defined as a ratio of fluxes in the direction of the GC and AC. The fluxes are calculated within solid angles limited by angle θ with the line connecting the Sun and GC. Anisotropy is given for three density profiles: $(\alpha,\beta,\gamma)=(2,2,0)$: ''isothermal'' curve, (2,3,0.2): ''best fit'' curve, and (1,3,1): for numerical simulation shape. The solid lines correspond to $r_0=5$ kpc and the dashed lines to $r_0=10$ kpc.

tional data at $E_\gamma \sim 10^{10}$ GeV, the fluxes are the same in all three cases. The corresponding values of $\dot{n}_0^h$ are 6.3×10^{-42} cm^{-3} s^{-1}, 1.3×10^{-41} cm^{-3} s^{-1}, and 1.6×10^{-41} cm^{-3} s^{-1}, respectively. These values also normalize, through relation Eq. (7), the flux of extragalactic protons, given by Eq. (4). The obtained results do not significantly differ from those in [25]. The photon flux is greater than the proton flux by a factor of 6.

Another signature of this model is the anisotropy caused by asymmetric position of the Sun in the galactic halo [26]. The anisotropy reveals itself most significantly as the large ratio of fluxes in the directions of the galactic center (GC) and the galactic anticenter (GA). We define the anisotropy $A(\theta)$ as this ratio with the fluxes measured within a solid angle limited by angle θ with the line connecting the Sun and the GC. This can be readily calculated using the distribution of the sources in the halo given by Eq. (9).

The anisotropy $A(\theta)$ is plotted in Fig. 5 as a function of θ for all three density profiles given by Eq. (9) with $r_0=5$ kpc (solid curves) and $r=10$ kpc (dashed curves). The estimated anisotropy is relevant for energies $E>1\times10^{10}$ GeV, where the contribution of the isotropic lower-energy component is small.

There is one more signature for this model, given by a direct flux of protons from the Virgo cluster, provided that they are weakly deflected by magnetic fields in the local supercluster (see [25]). Note that UHE photons from this source are absorbed, and cascade radiation does not propagate rectilinearly because of the cascade electron deflection in the magnetic field.

vi. Vortons. Vortons are charge and current carrying loops of superconducting string stabilized by their angular momentum [41]. Although classically stable, vortons decay by gradually losing charge carriers through quantum tunneling. Their lifetime, however, can be greater than the present age of the universe, in which case the escaping X particles will produce a flux of cosmic rays. The X-particle mass is set by the energy scale η_X of string superconductivity.

The number density of vortons formed in the early universe is rather uncertain. According to the analysis in Ref. [58], vortons are overproduced in models with $\eta_X > 10^9$ GeV, so all such models have to be ruled out. In that case, vortons cannot contribute to the flux of UHECR. However, an alternative analysis [59] suggests that the excluded range is 10^9 GeV$<\eta_X<10^{12}$ GeV, while for $\eta_X \gg 10^{12}$ GeV vorton formation is strongly suppressed. This allows a window for potentially interesting vorton densities with[3] $\eta_X \sim 10^{12}-10^{13}$ GeV. Production of UHE particles by decaying vortons was studied in Ref. [60]. As we already mentioned above, vortons cluster in the galactic halo and the discussion in the preceding subsection is therefore directly applicable to this case as well.

V. DISCUSSION

We studied observational constraints on various TD models, as well as possible signatures of TD as sources of the observed UHE radiation ($E \geqslant 10^{10}$ GeV).

The most stringent constraint is due to electromagnetic cascades. It depends on the energy spectrum of particles from decays and on astrophysical quantities which determine the development of the cascade (most notably on the flux of intergalactic infrared/optical radiation and on intergalactic magnetic field). The SUSY-QCD spectrum makes the cascade constraint weaker, because this spectrum predicts less higher energy particles and more low energy particles as compared with ordinary QCD spectrum. In case of very large m_X it means that for a given UHECR flux, less energy is transferred to the e-m cascade radiation. There are considerable uncertainties in the extragalactic flux of infrared radiation and extragalactic magnetic field. The conservative limit on the energy density of the cascade radiation imposed by the latest EGRET data is $\omega_{cas} \approx 2\times10^{-6}$ eV/cm^3. It could be $(3-5)\times10^{-6}$ eV/cm^3 with astrophysical uncertainties mentioned above. The further progress in the study of origin of EGRET extragalactic flux and in calculation of SUSY-QCD spectrum, in the pessimistic case, can exclude such TD as, e.g., necklaces as the sources of observed UHECR.

Another important constraint arises from the fact that at ultrahigh energies, the proton attenuation length $R_p(E)$ and the photon absorption length $R_\gamma(E)$ are both small compared to the Hubble radius. Models in which the typical distance between defects is $D \gg R_p$ are disfavored. In such models, the observed spectrum would have an exponential cutoff, unless a source is accidentally close to the observer. In the latter case the flux would be strongly anisotropic.

[3]These numbers assume that strings are formed in a first-order phase transition and that η_X is comparable to the string symmetry breaking scale η_s. For a second-order phase transition, the forbidden range widens and the allowed window moves towards higher energies [59].

Finally, in many cases TD give UHECR fluxes lower than the observed ones. We showed here that this is the case for monopole-string networks. Superconducting and ordinary cosmic strings probably belong to this category as well, although some loopholes still remain to be closed.

With all these constraints taken into account, it appears that only necklaces, monopolonium and relic SH particles survive as potential UHE sources.

The most important observational signature of TD as sources of UHE CR is the presence of photon-induced EAS. For all known mechanisms of UHE particle production the pions (and thus photons) dominate over nucleons. At energies lower than 1×10^{12} GeV, protons have considerably larger attenuation length than photons and the observed proton flux can be dominant. Nevertheless, even in this case photons reach an observer from sources located inside the sphere of radius $R_\gamma(E)$ (assuming that $R_\gamma>D$). Unlike protons, photons propagate rectilinearly, indicating the direction to the sources.

Necklaces with a large value of $r=m/\mu d>10^7$ have a small separation $D<R_\gamma$. They are characterized by a small fraction, R_γ/R_p, of photon-induced EAS at energies $10^{10}-10^{11}$ GeV. This fraction increases with energy and becomes considerable at the highest energies. For smaller values of $r\sim10^4-10^6$, when the separation is larger than R_γ but still smaller than R_p, most of UHE particles are expected to be protons (with a chance of incidental proximity of a source, seen as a direct gamma-ray source). Thus, in all cases necklaces are characterized by an excess of proton-induced showers. However, some fraction of photon-induced showers is always present, and it can be large at the highest energies.

Monopolonium, decaying vortons *and SH relic particles* are characterized by an enhanced density in the galactic halo. They give a photon-dominated flux without a GZK cutoff. Because of the asymmetric position of the Earth in the Galaxy, this flux is anisotropic. The largest flux is expected from the direction of the galactic center, where the density of sources is the largest. Unfortunately, the galactic center is not seen by gigantic arrays, such as Akeno, Fly's Eye, Haverah Park, and Yakutsk array. However, these detectors can observe a minimum in the direction of the galactic anticenter in particles with energies $E>1\times10^{10}$ GeV, as compared with the direction perpendicular to the galactic plane.

A flux from the Virgo cluster might be another signature of this model.

The search for photon induced showers is not an easy experimental task. It is known (see, e.g., Ref. [61]) that in the UHE photon-induced showers the muon content is very similar to that in proton-induced showers. However, some difference in the muon content between these two cases is expected and may be used to distinguish between them observationally. A detailed analysis would be needed to determine this difference.

The Landau-Pomeranchuk-Migdal (LPM) effect [62] and the absorption of photons in the geomagnetic field are two other important phenomena which affect the detection of UHE photons [61,63]; (see [21] for a recent discussion). The LPM effect reduces the cross-sections of electromagnetic interactions at very high energies. However, if the primary photon approaches the Earth in a direction characterized by a large perpendicular component of the geomagnetic field, the photon is likely to decay into electron and positron [61,63]. Each of them emits a synchrotron photon, and as a result a bunch of photons strikes the Earth atmosphere. The LPM effect, which strongly depends on energy, is thus suppressed. If on the other hand a photon moves along the magnetic field, it does not decay, and LPM effect makes shower development in the atmosphere very slow. At extremely high energies the maximum of the showers can be so close to the Earth surface that it becomes ''unobservable'' [21].

We suggest that for all energies above the GZK cutoff the showers be analyzed as candidates for being induced by UHE photons, with the probability of photon splitting in the geomagnetic field determined from the observed direction of propagation, and with the LPM effect taken into account. The search for photon-induced showers can be especially effective in the case of Fly's Eye detector which can measure the longitudinal development of EAS. The future Auger detector will have, probably, the highest potentiality to resolve this problem.

ACKNOWLEDGMENTS

We thank Michael Kachelriess for help in the calculations and Motohiko Nagano for information and interesting discussions. We are grateful to Svetlana Grigorieva for providing us with the results of her recent new calculations (unpublished) of proton energy losses and the values of $db(E)/dE$ used in Eq. (6). A.V. is grateful to Anne Davis and Paul Shellard for a discussion on vortons. We also thank Guenter Sigl for a valuable remark and Pijushpani Bhattacharjee for discussions. The work of A.V. was supported in part by the National Science Foundation. P.B. was supported by INFN at the University of Chicago.

APPENDIX A: UHE PARTICLE PRODUCTION DUE TO MULTIPLE LOOP FRAGMENTATION

We shall adopt the following simple model of loop fragmentation (It is somewhat similar to the model introduced in Ref. [51]). Each loop fragments into (N_1+1) daughter loops after it radiated away a fraction $(1-f_1)$ of its energy. The Lorentz factor of the daughters in the center-of-mass frame of the parent loop is Γ_1. If the initial mass of the loop is M, then after n rounds of fragmentation, the number of daughters is

$$N_n\sim N_1^n, \tag{A1}$$

and their energy, rest mass and Lorentz factor are, respectively,

$$E_n\sim(f_1/N_1)^nM, \tag{A2}$$

$$M_n\sim(f_1/N_1\Gamma_1)^nM, \tag{A3}$$

$$\Gamma_n\sim\Gamma_1^n. \tag{A4}$$

The fragmentation process stops at round n_* when $M_{n_*} \sim \eta$, where η is the symmetry breaking scale of strings, that is, when the size of the fragments becomes comparable to the string thickness,

$$n_* \sim \frac{\ln(M/\eta)}{\ln(N_1\Gamma_1/f_1)}. \tag{A5}$$

Loops decaying at the present time t_0 have masses $M \sim 10^2 G\mu^2 t_0$ and

$$M/\eta \sim 10^{55}\eta_{16}^3, \tag{A6}$$

where $\eta_{16} \equiv \eta/10^{16}$ GeV. The typical values of f_1, N_1, and Γ_1 are not known. Numerical simulations of loop fragmentation in Ref. [52] found $N_1 \sim 3-10$ and $\Gamma_1 \sim 1.3$. However, these simulations used loops of arbitrary shape, and the parameter values for loops in a realistic network may be quite different. It seems reasonable to assume that on average the loop has to lose at least 30% of its energy to initiate the next round of fragmentation, that is, $f_1 < 0.7$. As we shall see from Eq. (A9), the energy output of loops in the form of cosmic rays is maximized for the largest possible values of N_1 and f_1. In the estimates below, we shall adopt $N_1 \sim 10$, $f_1 \sim 0.7$, and $\Gamma_1 \sim 1.3$. The values of N_1 and f_1 appear somewhat large, and we shall keep in mind that we have made a rather optimistic choice of the parameters. With these values,

$$n_* \approx 44 + \ln\eta_{16}. \tag{A7}$$

Each fragmenting loop gives $\sim N_1$ particles of energy $\sim \eta\Gamma_1$ in the rest frame of the loop (~ 1 particle per intersection). The fraction F of the total energy of the initial loop that ends up in the form of UHE particles can be estimated as

$$F \sim \frac{\eta}{M}\sum_{n=1}^{n_*} N_n\Gamma_n. \tag{A8}$$

The dominant contribution to the sum is given by the last term (that is, by the last round of fragmentation), and we can write

$$F \sim \frac{\eta}{M}(N_1\Gamma_1)^{n_*} \sim f_1^{n_*}, \tag{A9}$$

where in the last step we have used the definition of n_*. Using Eq. (A7) and $f_1 \approx 0.7$, we have for the fraction of energy transferred to X particles

$$F \sim 2\times 10^{-7}\eta_{16}^{-0.4}. \tag{A10}$$

Most of the particles are emitted at energies

$$E_X \sim \Gamma_1^{n_*}\eta \sim 9\times 10^{20}\eta_{16}^{0.7}\ \text{GeV}. \tag{A11}$$

The X-particle injection rate is given by

$$\dot{n}_X \sim F\frac{\mu}{E_X t_0^3} \sim 3\times 10^{-55}\eta_{16}^{0.9}\ \text{cm}^{-3}\,\text{s}^{-1}. \tag{A12}$$

To maximize the diffuse proton flux, $I_p(E)$, we shall assume a power-law fragmentation function KE_r^{-p} with $p=1.5$ in the system where the X particle is at rest. After simple calculations using the Lorentz-transformation to the laboratory system, one obtains the diffuse flux as

$$I_p(E) = \frac{(2-p)f_N}{4\pi p}\frac{\dot{n}_X}{E_X}\left(\frac{E}{E_X}\right)^{-p} R_p(E), \tag{A13}$$

where $R_p(E)$ is the proton attenuation length. For $E = 6.3\times 10^{19}$ eV, using Eqs. (A11),(A12), we obtain $E^3 I_p(E) \approx 3\times 10^{18}\eta_{16}^{1.25}$ eV^2 m^{-2} s^{-1} sr^{-1} to be compared with the observed value 3×10^{24} eV^2 m^{-2} s^{-1} sr^{-1}. Thus the calculated flux is too small by a factor of 10^6. This discrepancy is difficult to resolve by stretching the range of the parameters f_1 and N_1. For example, with $f_1 \sim 0.9$ (which appears unreasonably large), the proton flux is $E^3 I_p(E) \approx 3\times 10^{23}\eta_{16}^{1.5}$ eV/m^2 s sr, but the cascade energy density is too large due to increase of E_X:

$$\omega_{cas} \approx (1/2)E_X\dot{n}_X t_0 \approx 7.4\times 10^{-3}\eta_{16}^{1.9}\ \text{eV/cm}^3.$$

We next consider particle production by cusp evaporation in the fragmenting loops. Assuming that cusps are periodically repeated and completely ''evaporated'' into particles, the energy rate of particle production (in the rest frame of the loop) is [35]

$$\dot{\mathcal{E}}_p \sim \mu\left(\frac{M}{\eta}\right)^{-1/3}. \tag{A14}$$

Compared to the gravitational radiation power, $\dot{\mathcal{E}}_g \sim 10^2 G\mu^2$, this is

$$\dot{\mathcal{E}}_p/\dot{\mathcal{E}}_g \sim 10^{-2}(G\mu)^{-1}\left(\frac{M}{\eta}\right)^{-1/3}. \tag{A15}$$

The Lorentz factor at the cusp is

$$\Gamma_c \sim \left(\frac{M}{\eta}\right)^{1/3}. \tag{A16}$$

The fraction of energy lost by a fragmenting loop in the form of particles is

$$F = 10^{-2}(G\mu)^{-1}(1-f_1)\sum_{n=0}^{n_c} N_n\frac{E_n}{M}\left(\frac{M_n}{\eta}\right)^{-1/3} \tag{A17}$$

$$= 10^{-2}(G\mu)^{-1}(1-f_1)\left(\frac{M}{\eta}\right)^{-1/3}\sum_{n=0}^{n_c}(f_1^2 N_1\Gamma_1)^{n/3}, \tag{A18}$$

where

$$n_c \sim 32 + 3\ln\eta_{16} \tag{A19}$$

is the value of n at which $\dot{\mathcal{E}}_p \sim \dot{\mathcal{E}}_g$.

For our choice of parameters, $f_1^2 N_1 \Gamma_1 > 1$ and the dominant contribution to Eq. (A18) is given by $n \sim n_c$. Then

$$F \sim (1-f_1) f_1^{n_c} \sim 3 \times 10^{-6} \eta_{16}^{-1}, \tag{A20}$$

which is comparable to Eq. (A10). The energy of the emitted particles is

$$E_X \sim \eta \Gamma_1^{n_c} \Gamma_c \sim 4 \times 10^{23} \eta_{16}^{-0.2} \text{ GeV}. \tag{A21}$$

This energy is too high: the observed flux cannot be obtained for any reasonable value of η without violating the cascade bound.

[1] N. Hayashida *et al.*, Phys. Rev. Lett. **73**, 3491 (1994); D. J. Bird *et al.*, Astrophys. J. **424**, 491 (1994).
[2] C. T. Norman, D. B. Melrose, and A. Achterberg, Astrophys. J. **454**, 60 (1995).
[3] P. L. Biermann, Max-Plank-Institut für Radioastronomie, Report No 731 (1997).
[4] V. S. Berezinsky, S. V. Bulanov, V. A. Dogiel, V. L. Ginzburg, and V. S. Ptuskin, *Astrophysics of Cosmic Rays* (Elsevier, Amsterdam, 1990), Chap. 4.
[5] M. Vietri, Astrophys. J. **453**, 863 (1995).
[6] E. Waxman, Phys. Rev. Lett. **75**, 386 (1995).
[7] M. Hoshino, J. Arons, Y. A. Gallant, and A. B. Langdon, Astrophys. J. **390**, 454 (1992).
[8] A. Vilenkin and E. P. S. Shellard, *Cosmic Strings and Other Topological Defects* (Cambridge University Press, Cambridge, England, 1994); M. B. Hindmarsh and T. W. B. Kibble, Rep. Prog. Phys. **55**, 478 (1995).
[9] K. Greisen, Phys. Rev. Lett. **16**, 748 (1966); G. T. Zatsepin and V. A. Kuzmin, Pis'ma Zh. Eksp. Teor. Fiz. **4**, 114 (1996).
[10] V. S. Berezinsky and G. T. Zatsepin, Phys. Lett. **28B**, 423 (1968).
[11] J. Bordes *et al.*, Astropart. Phys. **8**, 135 (1998).
[12] D. J. H. Chung, G. R. Farrar, and E. W. Kolb, astro-ph/9707036.
[13] V. Berezinsky and M. Kachelriess, Phys. Lett. B **422**, 163 (1998).
[14] T. J. Weiler and T. W. Kephart, Nucl. Phys. B (Proc. Suppl.) **51**, 218 (1998).
[15] S. Bonazzola and P. Peter, Astropart. Phys. **7**, 161 (1997).
[16] F. A. Aharonian, P. Bhattacharjee, and D. N. Schramm, Phys. Rev. D **46**, 4188 (1992).
[17] G. Sigl, D. N. Schramm, and P. Bhattacharjee, Astropart. Phys. **2**, 401 (1994).
[18] V. S. Berezinsky, Sov. J. Nucl. Phys. **11**, 399 (1970).
[19] R. J. Protheroe and P. L. Biermann, Astropart. Phys. **6**, 45 (1996).
[20] EGRET Collaboration, P. Sreekumar *et al.*, Astrophys. J. **494**, 523 (1998).
[21] R. Protheroe and T. Stanev, Phys. Rev. Lett. **77**, 3708 (1996); **78**, 3420(E) (1997).
[22] G. Sigl, astro-ph/9611190.
[23] V. Berezinsky, Nucl. Phys. **B380**, 478 (1992).
[24] P. Bhattacharjee, C. T. Hill, and D. N. Schramm, Phys. Rev. Lett. **69**, 567 (1992).
[25] V. Berezinsky, M. Kachelriess, and A. Vilenkin, Phys. Rev. Lett. **79**, 4302 (1997).
[26] S. L. Dubovsky and P. G. Tinyakov, hep-ph/9802382.
[27] Yu. L. Dokshitzer, V. A. Khose, A. H. Mueller, and S. I. Troyan, *Basics of Perturbative QCD* (Editions Frontières, Gif-sur-Yvette, France, 1991).
[28] V. Berezinsky and M. Kachelriess, hep-ph/9803500.
[29] M. Birkel and S. Sarkar, hep-ph/9804285.
[30] V. Berezinsky and S. Grigorieva, Astron. Astrophys. **199**, 1 (1988).
[31] A. V. Kravtsov, A. K. Klypin, J. S. Bullock, and J. R. Primack, astro-ph/9708176.
[32] J. F. Navarro, C. S. Frenk, and S. D. M. White, Astrophys. J. **462**, 563 (1996).
[33] C. T. Hill, D. N. Schramm, and T. P. Walker, Phys. Rev. D **36**, 1007 (1987).
[34] P. Bhattacharjee and N. C. Rana, Phys. Lett. B **246**, 365 (1990).
[35] R. Brandenberger, Nucl. Phys. **B293**, 812 (1987); J. H. MacGibbon and R. H. Brandenberger, *ibid.* **B331**, 153 (1990).
[36] T. Vachaspati and A. Vilenkin, Phys. Rev. D **35**, 1131 (1987).
[37] V. Berezinsky, X. Martin, and A. Vilenkin, Phys. Rev. D **56**, 2024 (1997).
[38] V. Berezinsky and A. Vilenkin, Phys. Rev. Lett. **79**, 5202 (1997).
[39] C. T. Hill, Nucl. Phys. **B224**, 469 (1983).
[40] P. Bhattacharjee and G. Sigl, Phys. Rev. D **51**, 4079 (1995).
[41] R. L. Davis and E. P. S. Shellard, Phys. Lett. B **209**, 485 (1988); Nucl. Phys. **B323**, 209 (1989).
[42] V. A. Kuzmin and V. A. Rubakov, Talk at the Workshop ''Beyond the Desert,'' Castle Rindberg, 1997, astro-ph/9709187.
[43] V. Kuzmin and I. Tkachev, hep-ph/9802304.
[44] K. Benaki, J. Ellis, and D. Nanopoulos, hep-ph/9803333.
[45] P. H. Frampton, B. Keszthelyi, and N. J. Ng, astro-ph/9709080.
[46] J. P. Ostriker, C. Thompson, and E. Witten, Phys. Lett. B **180**, 231 (1986).
[47] V. Berezinsky and H. Rubinstein, Nucl. Phys. **B323**, 95 (1988).
[48] V. Berezinsky and A. Vilenkin (in preparation).
[49] E. P. S. Shellard, Nucl. Phys. **B283**, 624 (1987).
[50] A. J. Gill and T. W. B. Kibble, Phys. Rev. D **50**, 3660 (1994).
[51] C. J. Hogan and M. J. Rees, Nature (London) **311**, 109 (1984).
[52] R. J. Scherrer and W. H. Press, Phys. Rev. D **39**, 371 (1989).
[53] G. R. Vincent, N. Antunes, and M. Hindmarsh, Phys. Rev. Lett. **80**, 2277 (1998).
[54] G. R. Vincent, M. Hindmarsh, and M. Sakellariadou, Phys. Rev. D **56**, 637 (1997).
[55] P. Bhattacharjee, Phys. Rev. D **40**, 3968 (1989).

[56] V. Berezinsky and S. Grigorieva, *Proceedings of the 16th International Cosmic Ray Conference*, Kyoto, 1976, Vol. 2, p. 81.

[57] P. L. Biermann and P. A. Strittmatter, Astrophys. J. **322**, 643 (1987); W. H. Ip and W. I. Axford, in *Astrophysical Aspects of Most Energetic Cosmic Rays*, edited by M. Nagano (World Scientific, Singapore, 1991), p. 273; J. P. Rachen and P. L. Biermann, Astron. Astrophys. **272**, 161 (1993).

[58] R. Brandenberger, B. Carter, A.-C. Davis, and M. Trodden, Phys. Rev. D **54**, 6059 (1996).

[59] C. J. A. P. Martins and E. P. S. Shellard, hep-ph/9806480.

[60] L. Maspieri and G. Silva, Astropart. Phys. **8**, 173 (1998).

[61] F. A. Aharonian, B. L. Kanevsky, and V. A. Sahakian, J. Phys. G **17**, 1909 (1991).

[62] L. D. Landau and I. Pomeranchuk, Dokl. Akad. Nauk SSSR **92**, 535 (1953); A. B. Migdal, Phys. Rev. **103**, 1811 (1956).

[63] K. Kasahara, in *Proceedings of International Symposium on ''Extremely High Energy Cosmic Rays: Astrophysics and Future Observatories,''* Tanashi, Tokyo, Japan, 1996, edited by M. Nagano (Institute for Cosmic Ray Research, University of Tokyo, 1996), p. 221.